Materials Science-Poland, Vol. 22, No. 4, 2004

Manipulation of electron spin in a quantum dot using a magnetic field and voltage gates

D. GIULIANO[1, 2], P. LUCIGNANO[1, 3], A. TAGLIACOZZO[1, 3*]

[1]Coherentia – INFM (Istituto Nazionale di Fisica della Materia), Unità di Napoli

[2]INFN and Dipartimento di Fisica Università di Calabria, Arcavacata di Rende, Italy

[3]Dipartimento di Scienze Fisiche Università di Napoli "Federico II", Napoli, Italy

In this paper, we show that it is possible to manipulate the many-body wave function of an isolated dot with a few electrons by locally applying magnetic and electric fields. We polarize the dot at a level crossing, where the sensitivity is at its maximum. Time-dependent fields produce a superposition of the states involved in the avoided crossing. In the case of $N = 2$ and $N = 3$ electrons, the results of exact diagonalisation give information about the nature of these states and allow us to construct an effective Hamiltonian describing the coupling. The formalism for evaluating the Berry phase arises naturally. We argue that a quantum dot, capacitively coupled to a quantum point contact, can influence its conductance. The quantum superposition of the states produced by cycling the fields on the dot can be measured this way.

Key words: *quantum transport device; quantum dot; Berry phase; qubits*

1. Introduction

Manipulating the phase of a quantum electronic system in a controlled fashion is presently one of the challenges of nanophysics, especially in view of its possible applications in quantum computing [1]. The most promising route to achieve such a task is probably provided by coherent solid-state devices. For instance, a superconducting Josephson qubit has already been realized as the Cooper pair box, namely a small superconducting island weakly coupled to a charge reservoir via the Josephson junction [2]. The quantum state of the box can be tuned to a coherent superposition of the charge-zero and charge-one states. The possibility of realizing superpositions of flux states has been considered as well [3]. Entanglement in semiconducting devices made of two quantum dots (QD), one on top of each other ("quantum dot molecule") has recently been optically measured, and double dots have been inserted into a transport device [4]. Double QD have been proposed as possible qubits [5]. The state of a QD

*Corresponding author, e-mail: Arturo.Tagliacozzo@na.infn.it.

can be finely tuned by means of external magnetic and electric fields or by changing the coupling between the dot and the contacts [6].

Quantum algorithms usually assume that either the system dynamically evolves through a sequence of unitary transformations or that a set $\vec{\lambda}$ of external control parameters of the Hamiltonian H smoothly changes in time ("adiabatic evolution") [7]. Accidental level degeneracies are quite common in QD's, which is seen both theoretically and experimentally [8]. In this work, we show that they can be used to add a Berry phase to the dot and to manipulate it. In fact, if adiabatic evolution is realized across a closed path γ in parameter space close enough to an accidental level degeneracy, the nontrivial topology of the Hilbert space makes the state of the system take up a "geometrical" phase Γ, referred to as the "Berry phase" [9]. The value of Γ may be controlled by properly choosing γ.

Here we discuss the case of a vertical dot with a few electrons in a rather strong orthogonal magnetic field B. By increasing B, the energy levels undergo crossings to higher angular momenta states and spin states. We will show that the Rashba spin -orbit perturbing term, implemented by polarizing a voltage gate on top of an isolated dot, can turn one of these crossings into an anticrossing by mixing states of different quantum numbers and opening a gap. Cycling the voltage in an appropriate way allows an $SU(2)$ Berry phase to be added to the many body wave function of the electrons in the dot. This phase could be monitored by means of transport measurement.

In Chapter 2 we set up a model for a vertical QD with a few interacting electrons based on exact diagonalisation results and describe the crossover to the state with maximum spin and maximum angular momentum. The effect of the Rashba spin-orbit (SO) term on the ground state of the system is discussed. In Chapter 3 we concentrate on the case where $N = 2$. There is an avoided crossing at the singlet–triplet transition [10] which can be described by an equivalent Hamiltonian $\tilde{H}$ involving just one effective spin $\tilde{S} = 1/2$. We shall make the state of the system evolve in time by means of a time-dependent SO coupling, which could be implemented by a microwave driven gate voltage. The spin state is shown to acquire the usual SU(2) Berry phase. In Chapter 4 we argue that a dot with $N = 3$ electrons gives the chance of producing an SU(3) Berry phase. In order o perform a nontrivial γ circuit, however, there are too many parameters to control. This makes the realization of a full SU(3) Berry phase unrealistic at the present time. Nevertheless, we show that a simpler setup can be imagined based on a three-level avoided crossing and that this setup allows further phase manipulation. The final chapter collects comments on possible methods for reading out the added phase.

2. Vertical quantum dot with azimuthal symmetry

We consider an isolated, vertical QD, disk-shaped in the (x,y)-plane (θ and ρ are the polar coordinates in the plane). An external static magnetic field B and electric field E are applied along the z-axis. The dot's Hamiltonian H_D adiabatically depends on these external parameters, generically referred to as $\vec{\lambda}$ in the following. The dot's Hamiltonian is

$$H_D = H_{0D} + \mu \sum_i l_i^z B + \frac{1}{2}\hbar\omega_c(B)\sum_i \sigma_i^z + \frac{\alpha}{\hbar}\sum_i \left(\vec{E}\times\vec{\pi}_i\right)\cdot\vec{\sigma}_i \qquad (1)$$

where H_{0D} includes the confining parabolic potential of frequency ω_d and the Coulomb interaction $U(B,\omega_d)$. $\omega_c(B) = eB/m^*_c$ is the cyclotron frequency. The second and third terms at the r.h.s. of Eq. (1) are the orbital and spin Zeeman terms, respectively. The $\vec{l}_i$ are the components of the electron angular momentum orthogonal to the dot disk, and μ is the electronic magnetic moment $\mu = e\hbar/(2m^*c)$. The last term is the spin-orbit (Rashba) term with a coupling constant $\alpha \propto \vec{E}$, which has the dimension eV·Å. The generalized momentum is $\vec{\pi}_i = \vec{p}_i + (e/c)\vec{A}(r_i)$, where $\vec{p}_i$ is the linear momentum of particle *i* and $\vec{A}$ is the vector potential due to the magnetic field *B*. In a symmetric gauge it takes the form $\vec{A} = B/2\,(-y, x, 0)$. From now on we neglect the Zeeman spin splitting, since it only lifts the spin degeneracy. The orbital wave function for an electron in a two-dimensional harmonic confining potential and an external *B* field along $\hat{z}$ is

$$\Psi_{n,m}(\rho,\theta) = \frac{e^{im\theta}}{l\sqrt{\pi}} R_{n|m|}(t), \qquad (2)$$

where *n*, *m* are the orbital quantum numbers, $t = \rho^2/l^2$, and $l = \sqrt{\hbar/m^*\omega_0}$ ($\omega_0 = \sqrt{\omega_d^2 + \omega_c^2(B)/4}$). The radial wave function in Eq. (2) is expressed in terms of the Laguerre polynomials L_ν^μ as

$$R_{n|m|}(t) = C_{n|m|}\, e^{-1/2}\, t^{|m|/2}\, L^{|m|}_{(n-|m|)/2}(t); \qquad C_{n|m|} = \left[\frac{\left(\frac{n-|m|}{2}\right)!}{\left(\frac{n+|m|}{2}\right)!}\right]^{\frac{1}{2}} \qquad (3)$$

We label the single electron states in the dot by $|n, m, s = 1/2, s^z>$ (s, s^z are the electron spin and *z*-component).

In the absence of both interaction and magnetic field, the lowest lying single particle states are occupied with minimum spin. The GS Slater determinant for $N = 5$ is sketched pictorially in Fig. 1a, where energy is plotted on the vertical axis. Each box represents a single particle state labelled by *n,m*, and each arrow represents the spin projection along the quantisation axis of the electron occupying the corresponding box.

In Figure 2 (left panels) we show the lowest lying total energy levels at a fixed angular momentum *M* versus *M* for $U = 13$ meV and three values of *B*. These are $B = 5$ meV (top), $B = B^* = 7$ meV (middle), and $B = 11.5$ meV (bottom).

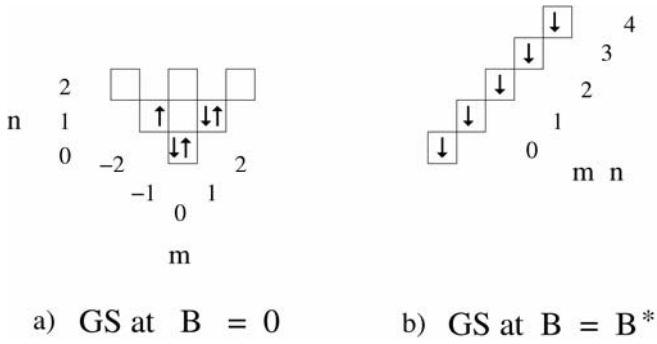

Fig. 1. The Slater determinants quoted in the text. Quantum numbers are $N = 5$, $S = 1/2$ for the state at $B = 0$ (a) and $S = 5/2$ for the state at $B = B^*$, which is the magnetic field at which the maximum absolute value of S is achieved (b)

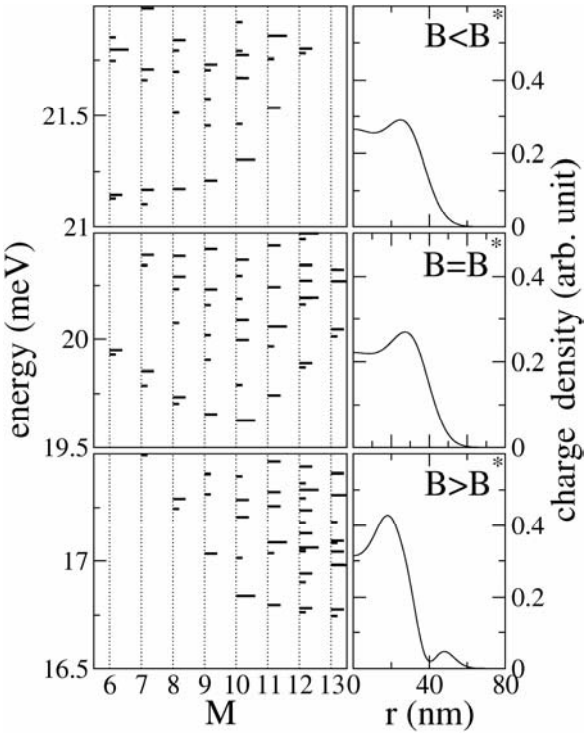

Fig. 2. Energy levels without SO coupling for a dot with $N = 5$ electrons at $U = 13$ meV and $\omega_d = 5$ meV. Magnetic field values are (in units of $\hbar\omega_c$): $B = 5$ meV (top), $B = B^* = 7$ meV (middle), $B = 11.5$ meV (bottom). Total M is on the x axis. Levels are drawn with short, medium, or long dashes, corresponding to the total spin: $S = 1/2$, $3/2$, $5/2$

This level structure, as well as the radial charge and spin densities, are calculated by exact diagonalisation using a basis of 28 single particle orbitals. Slater determinants are constructed and span the Hilbert space up to matrices ($10^5 \times 10^5$), depending

on the number of electrons. Unscreened Coulomb electron-electron interaction matrix elements are calculated analytically basing on the states given by Eq. (2).

At each M, the spin degeneracy is marked by dashes of different length: short dashes for S = 1/2 (doubly degenerate level), medium dashes for S = 3/2 (fourfold degeneracy), and long dashes for S = 5/2 (sixfold degeneracy). On the r.h.s. of the picture, the radial charge density of the corresponding GS is plotted vs. the distance r from the dot centre. Figure 2 (left panels) shows that the levels cross with increasing B when M or S increase. Electron-electron correlations imply that when M increases S also increases.

At $B = B^* = 7$ meV, the spin S reaches its maximum value of $S = N/2$. The largest contribution to the GS wave function is given by the Slater determinant depicted in Fig. 1b (for N = 5), corresponding to $M = \sum_0^{N-1} m = 10$. We concentrate on the state at $B = B^*$, namely the Fully Spin Polarized (FSP) GS. This corresponds to the "maximum density droplet" state discussed in literature [11]. Qualitatively we can say that at $B = B^*$ the dot has the smallest radius. As can be seen from the GS charge density, a further increase in B leads to the so-called reconstruction of the charge density of the dot. For $B > B^*$, the value of M for the GS increases, but S is no longer at its maximum. In the bottom panel of Fig. 2 it is shown that at B = 11.5 meV the GS energy is achieved for M = 13 with a doublet (S = 1/2) state. The corresponding charge density of the dot, depicted on the r.h.s., is strongly modified close to the edge [12]: it displays a node, followed by an extra non-zero annulus at a larger distance. In view of the fact that our expansion of the wave function includes only rotationally invariant components, the breaking of azimuthal symmetry is impossible. By contrast, this is found to occur in density functional calculations, and the corresponding GS is referred to as the de Chamon-Wen phase [13]. The GS at $B = B^*$ can be compared with a FSP quantum Hall state of an extended disk in the absence of lateral confinement (Quantum Hall Ferromagnet (QHF) at a filling of one). Indeed, Fig. 1b resembles the occupancy of the lowest Landau level (LLL) up to a maximum $m = N - 1$, except that in our case the single particle levels corresponding to the LLL are not all degenerate in energy. In the language of the quantum Hall effect, the unperturbed levels are:

$$\varepsilon_{\nu,m} = (2\nu + |m| + 1)\hbar\omega_o - \frac{m}{2}\hbar\omega_c \tag{4}$$

where $\nu = (n - |m|)/2$ and $\omega_o = \sqrt{\omega_d^2 + \omega_c^2/4}$. The LLL is for $\nu = 0$ and $m \geq 0$. The Slater determinant for the LLL has a charge density that is flat as a function of r up to the disk edge, at which it rapidly falls to zero. In our case, this feature is lost due to U and the fact that the number of electrons is small.

We now add spin-orbit interaction to the dot. This can be tuned by applying an electric field E in the $\hat{z}$ direction, which couples the spin of the electrons in the dot.

At $E \neq 0$, the spin-orbit term couples states with opposite spin components: $s^z = \pm(1/2)$. The matrix elements can be easily calculated

$$H_{so} = \frac{\alpha}{l}\sum_{nn'}\sum_{m}\left\{B_{n'm+1,nm}\left(1-\frac{\omega_c}{\omega_0}\right)c^{\dagger}_{n'm+1\downarrow}c_{nm\uparrow} + A_{n'm-1,nm}\left(1-\frac{\omega_c}{\omega_0}\right)c^{\dagger}_{n'm-1\uparrow}c_{nm\downarrow}\right\}$$

with

$$A_{n',m',nm} = \delta_{m'+1,m}\int_0^{\infty} dt R_{n'|m'|}(t)\left(2\sqrt{t}\frac{\partial}{\partial t} + \frac{m}{\sqrt{t}}\right)R_{n|m|}(t)$$

and

$$B_{n',m',nm} = \delta_{m'-1,m}\int_0^{\infty} dt R_{n'|m'|}(t)\left(2\frac{\partial}{\partial t}^{\dagger}\sqrt{t} + \frac{m'}{\sqrt{t}}\right)R_{n|m|}(t) \qquad (5)$$

Here $B_{nm,n'm-1} = A^{*}_{n'm-1,nm}$, which implies that the Hamiltonian is hermitian. A pictorial sketch can help to understand what happens in the presence of both the orthogonal magnetic field and SO Rashba coupling. SO coupling tends to shift the $\downarrow$ spin density radially w.r.to the $\uparrow$ spin density. This is confirmed by plotting the occupation numbers $n_{nm\sigma} =< GS \mid c^{\dagger}_{nm\sigma}c_{nm\sigma} \mid GS >$ with $n = m$ (see Fig. 3 and [14]).

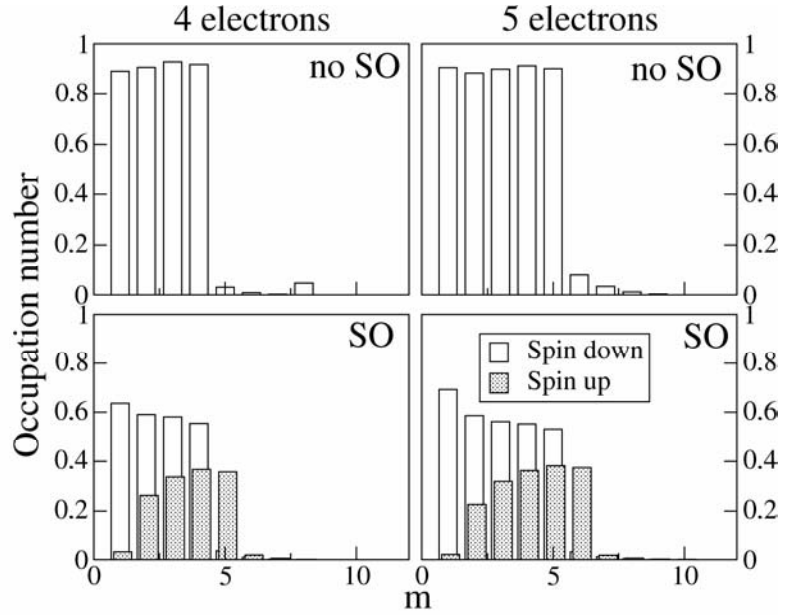

Fig. 3. Occupation numbers $n_{n=m,m,\sigma}$ in the *GS* with *N* 4 (5) electrons (left(right)), without SO (top) and with SO (α = 100 meVÅ) (bottom). Other parameters are: B = 7 meV, U = 13 meV, and ω_d = 5 meV. White bars refers to spin down, grey bars refer to spin up. The *FSP* GS of the dot with N = (4) 5 electrons has a total spin S = 2 (5/2) and a z-component of the total angular momentum J_z = 15/2

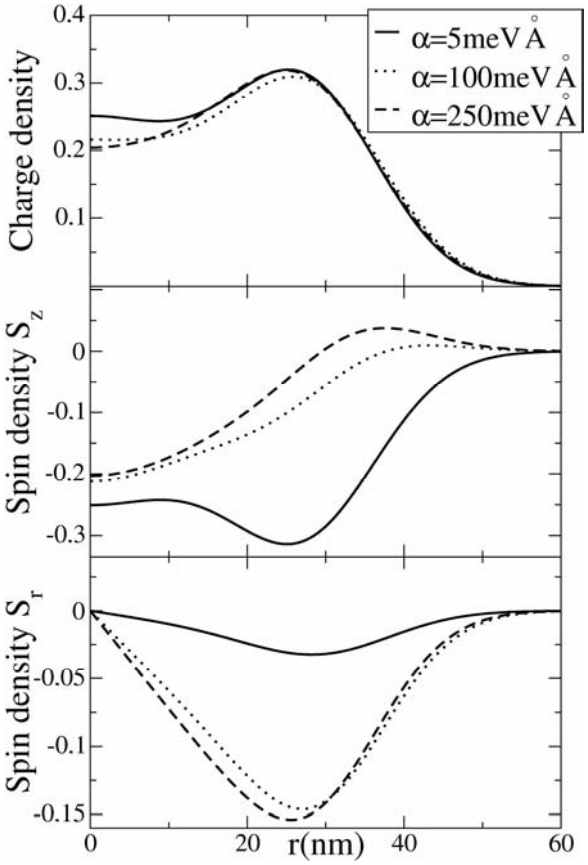

Fig. 4. Charge density, azimuthal spin density S_z, and radial in plane spin density S_r in the GS (N = 5, J = 15/2) at SO couplings α = 5, 100, 250 meV·Å. Here, B = 7 meV, U = 13 meV, and ω_d = 5 meV

The spin density is quite sensitive to the addition of SO up to the saturation. Now the z-component of the total spin is no longer a good quantum number and some mixing with down spin electrons appears. While s_z and m are no longer separately conserved, their sum $j_z = s_z + m$ (with j_z being a half integer) is still conserved. In result, the Rashba coupling acts as an effective in plane magnetic field that forces the precession of electron spins in the dot plane. The out of plane component of B tends to tilt spin out of the plane, acting oppositely to the Rashba coupling. Our calculation confirms the intuitive idea that SO coupling is weakened by an orthogonal magnetic field. Indeed, by increasing ω_c in Eq. (2), the strength of the SO interaction decreases. The z-component of spin density and its radial component for the GS with N = 5 and J_z = 15/2 for U = 13 meV are plotted vs. the distance from the dot centre in Fig. 4, for three different values of SO coupling. They are also compared to the charge density distribution. As it appears from Fig. 4 (top panel), the charge density of the GS is only mildly changed when we increase the SO coupling.

The SO interaction lifts the degeneracy of J_z. The multiplet with $N = 5$, $S = 5/2$, and $M = 10$ at $B = B^* = 7$ meV and $U = 13$ meV splits when the strength of SO coupling α is increased. The strength of U is responsible not only for the fact that the GS belongs to this multiplet, but also for the order in the sequence of energies: $J_z = 15/2$, 17/2, 19/2, 21/2, 23/2, 25/2 (from bottom to top). At small values of U, this sequence has the order $J_z = 25/2$, 23/2, 21/2, 19/2, 15/2, 17/2, as shown in Fig. 5. With increasing U, some level crossings occur. This crossing defines B^*, which is rather insensitive to SO coupling.

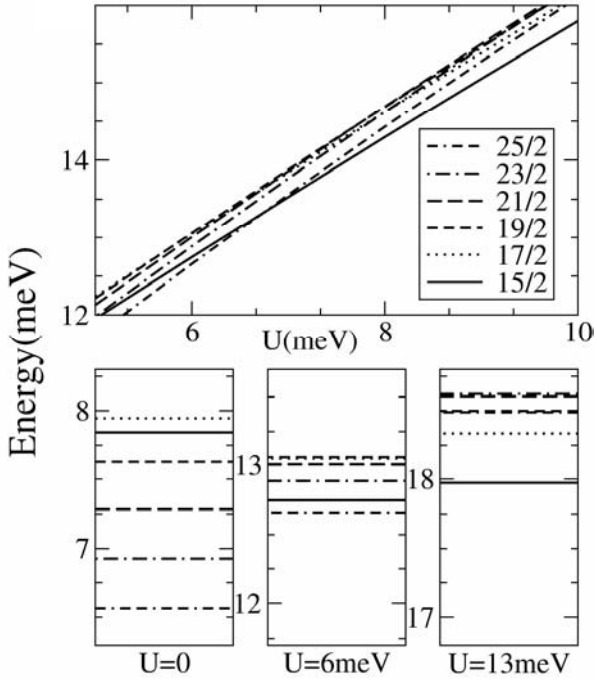

Fig. 5. Energy levels for $N = 5$, $B = 7$ meV, $\omega_d = 5$ meV, and $\alpha = 100$ meVÅ, for different values of U. In the upper panel the crossings that allow the *FSP* polarized state to be the ground state when U is large are shown. The order of the levels is magnified in the bottom panels for three different values of U

The order at three different values of U is magnified in the bottom panels of Fig. 5. The case for $U = 13$ meV is shown in the bottom right panel of Fig. 5 – the lowest state in energy is for $J_z = 15/2$, followed by $J_z = 17/2$, 19/2 (almost degenerate with 25/2), and 25/2, 21/2, 23/2. At $U = 13$ meV a sizeable gap is formed between the $J_z = 15/2$ GS and the first excited state $J_z = 17/2$. The other states of the multiplet are bunched together at higher energies.

We discuss the peculiarity of the first excited state elsewhere [15], which displays a spin texture with some analogies to the Skyrmion state of the QHF.

3. The $N = 2$ singlet–triplet avoided crossing

In this chapter, we consider two electrons ($N = 2$) only. In particular, B is tuned close to the singlet–triplet transition that occurs at $B = B^*$. In the absence of SO coupling, the states of a vertical dot are usually denoted as $|M, S, S^z>$, where M is the orbital angular momentum, S is the total spin, and S^z is its z-component [8]. The low -lying energy levels are reported vs. B and in the absence of SO in Fig. 1, to be compared with the ones when SO has been added.

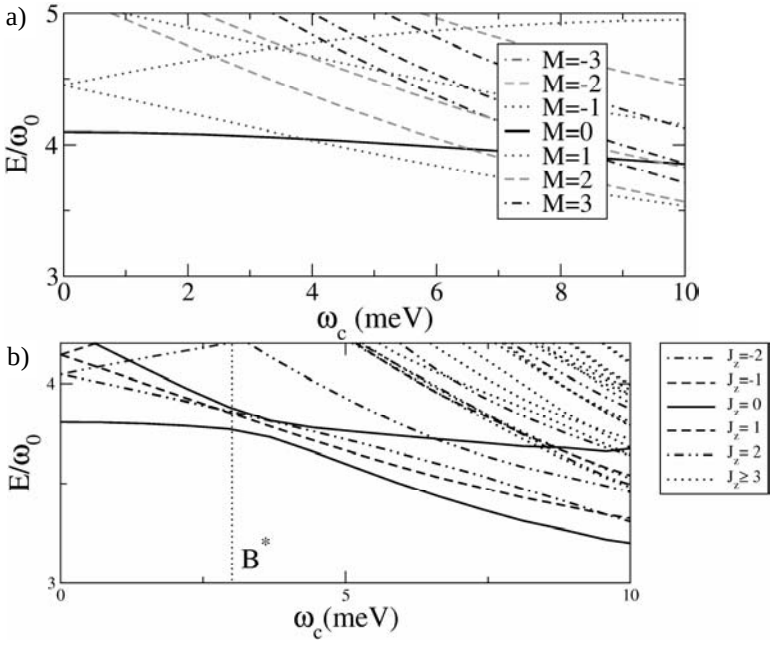

Fig. 6. A dot with $N = 2$ particles: energy spectrum vs. magnetic field ω_c in the absence of SO for $\omega_d = 5$ meV, and $U = 13$ meV (left box); energy spectrum vs. magnetic field ω_c in the presence of SO for the same parameters and $\alpha = 250$ meV·Å (right box)

The lowest lying singlet–triplet crossing is converted into an anticrossing. The Slater determinants that are involved the most corresponding to the states

$$|M=0,S=0,S_z=0>=d^{\dagger}_{-\downarrow}d^{\dagger}_{-\uparrow}|0>$$

$$|M=1,S=1,S_z=-1>=d^{\dagger}_{+\downarrow}d^{\dagger}_{-\downarrow}|0>$$

$$|M=1,S=1,S_z=0>=\frac{1}{\sqrt{2}}\left(d^{\dagger}_{+\uparrow}d^{\dagger}_{-\downarrow}+d^{\dagger}_{+\downarrow}d^{\dagger}_{-\uparrow}\right)|0>$$

$$|M=1,S=1,S_z=1>=d^{\dagger}_{+\uparrow}d^{\dagger}_{-\uparrow}|0> \qquad (6)$$

Here, $d^{\dagger}$ are creation operators for dot electrons and the label $-$ refers to the single particle orbital $n = 0$, $m = 0$, while the label $+$ represents $n = 1$, $m = 1$. As seen in Fig. 6, SO couples the first and second of these states, both of which belong to the total angular momentum $J = M + S_z = 0$ (the other two belong to $J_z = 1$ and $j_z = 2$, respectively).

We want to show that under some special circumstances the Hamiltonian close to B^* can be reduced to the one of Eq. (11). The Hilbert space spanned by the four states in Eq. (6) can be mapped onto a pseudospin representation in terms of two spins, 1/2: $\vec{S}_1$ and $\vec{S}_2$ and with the corresponding basis $|S_+, S_+^z>$, with $\vec{S}_{\pm} = \vec{S}_1 \pm \vec{S}_2$ [16]. A comparison of the matrix elements onto the basis space show that the following correspondence holds

$$P\sum_s d_{ns}^{\dagger} d_{n's} P \;\Rightarrow\; n\delta_{n,n'}\left[\vec{S}_1\cdot\vec{S}_2 - \frac{1}{4} + n\right]$$

$$P\sum_{ss'} d_{ns}^{\dagger}\frac{1}{2}\vec{\sigma}_{ss'} d_{n's'} P \;\Rightarrow\; \frac{1}{2}\delta_{n,n'}\vec{S}_+ + \delta_{n,-n'}\frac{1}{2\sqrt{2}}\left[\vec{S}_- + 2in\vec{T}\right] \tag{7}$$

where $\vec{T} = \vec{S}_1 \times \vec{S}_2$. P projects onto the Hilbert space of the four states. States $|S_+, S_+^z>$ are eigenstates of $\vec{S}_+$ and $\vec{S}_1\cdot\vec{S}_2$, while $\vec{S}_+$ and $\vec{T}$ produce transitions from the singlet state to triplets.

In this representation, the Hamiltonian close to $B = B^*$ takes the form:

$$H_{S_1,S_2} = K\vec{S}_1\cdot\vec{S}_2 - \mu B S_+^z + \frac{1}{2\sqrt{2}}\left[b_+\left(\vec{S}_-^{-} + 2in\vec{T}^{-}\right) + h.c.\right] \tag{8}$$

where $b_+ = \alpha/l$. The second term is the Zeeman splitting in the triplet and the first two terms account for crossing at B^*. SO, by coupling the singlet and triplet with $S_+^z = -1$, opens up a gap and produces the anticrossing observed in Fig. 1. It can be shown that while $\vec{S}_1\cdot\vec{S}_2$ and $\vec{S}_+$ commute, they do not commute with $\vec{S}_-$ and $\vec{T}$, nor do $\vec{S}_-$ and $\vec{T}$ commute with each other. This proves that SO couples the centre of mass coordinates with the relative ones. Hence, the Kohn's theorem does not apply and microwave radiation shed onto the dot probes interactions as well.

As seen in Fig. 6, SO does not couple the states $|1,1>$, $|1,0>$, $|0,0>$, and $|1,-1>$. As far as SO is concerned, they are frozen. If we retain only the two states involved in anticrossing, we can further simplify the problem to a single spin 1/2: $\tilde{S}$. The correspondence between states is $|0,0> \rightarrow |\uparrow>$ and $|1,-1> \rightarrow |\downarrow>$. Defining P' as the projector on the two state basis, we have

$$P'S_+^z P' \Rightarrow \tilde{S}^z - \frac{1}{2}; \qquad P'\vec{S}_1 \cdot \vec{S}_2 P' \Rightarrow -\tilde{S}^z - \frac{1}{4}$$

$$P'S_-^{\pm} P' \Rightarrow -\sqrt{2}\tilde{S}^{\pm}, \qquad P'T^{\pm} P' \Rightarrow \mp \frac{i}{\sqrt{2}}\tilde{S}^{\pm} \tag{9}$$

It follows that the effective Hamiltonian of Eq. (8), rewritten in the new representation, reads

$$H_{\tilde{S}} = -\frac{1}{2}\left(\frac{K}{2} - \mu B\right) - \vec{\tilde{b}} \cdot \vec{\tilde{S}} \tag{10}$$

where $\tilde{b}^z = K + \mu B$ and $\tilde{b}^{\pm} = 2b^{\pm}$. This maps the two-electron Hamiltonian of Eq. (1), close to the anticrossing point, onto the Hamiltonian

$$\hat{H}_{\tilde{S}} = -\vec{b} \cdot \vec{\tilde{S}} \equiv -\begin{bmatrix} b\cos\vartheta & b\sin\vartheta e^{i\omega t} \\ b\sin\vartheta e^{-i\omega t} & -b\cos\vartheta \end{bmatrix} \tag{11}$$

where

$$b = \sqrt{\omega_o^2 + \alpha^2/l^2}, \quad \tan\vartheta = \frac{\alpha}{\omega_o l} \quad (\text{or } b_z = b\cos\vartheta = \omega_o, \quad b_{\pm} = b\sin\vartheta e^{\pm i\omega t} = \frac{\alpha e^{\pm i\omega t}}{l})$$

and we have assumed an oscillating time dependence for the electric field

$$E \rightarrow E\, e^{\pm i\omega t}$$

The dot state may be controlled by properly tuning the external control parameters *B* and *E*. An adiabatic cycle is realized by keeping *B* fixed, and by slowly and periodically varying *E* with a time period *T*.

As the first step, we find the instantaneous eigenstates of $\hat{H}_{\tilde{S}}(t)$ in Eq. (11), corresponding to the eigenvalues $\varepsilon = \pm b$

$$|+,t\rangle = \begin{pmatrix} \cos\dfrac{\vartheta}{2} \\ \sin\dfrac{\vartheta}{2} e^{i\omega t} \end{pmatrix}, \qquad |-,t\rangle = \begin{pmatrix} -\sin\dfrac{\vartheta}{2} e^{-i\omega t} \\ \cos\dfrac{\vartheta}{2} \end{pmatrix} \tag{12}$$

The Berry phase accumulated by the states $|\pm>$, by adiabatically operating along a period *T*, is

$$\Gamma_{\pm}(T) = i\oint_{\gamma} d\vec{\lambda} \cdot \left\langle \pm, \vec{\lambda} \middle| \vec{\nabla}_{\vec{\lambda}} \middle| \pm, \vec{\lambda} \right\rangle \tag{13}$$

Here, $\vec{\lambda} \equiv \vec{b}$ is the set of parameters describing the system.

$$\frac{d\Gamma_{\pm}}{dt} = \mp\frac{\omega}{2}\left(1-\cos\left(\vartheta\right)\right) \Rightarrow \Gamma_{\pm}\left(t\right) = \mp\frac{\pi t}{T}\left(1-\cos\left(\vartheta\right)\right) \tag{14}$$

It is useful to fix the phases of the adiabatic basis $|\pm, t>$ in such a way that they satisfy the parallel transport condition between successive times, namely

$$<\pm, t|\frac{d}{dt}|\pm, t>=0 \tag{15}$$

This choice implies that non-adiabatic terms (i.e., terms of $O(1/T)$ are always off -diagonal. Let us choose such an initial condition that the spin $\tilde{S}$ is in the state $|+>$ with an energy of $-b$. In the basis of states $e^{-i\Gamma_{\pm}(t)}|\pm(t)>$, at later times the spin wave function takes the form:

$$|u(t)>=e^{-i\omega t/2}\begin{pmatrix} \cos bt - i\cos\vartheta\sin bt + i\dfrac{\omega}{2b}\sin bt \\ -i\sin\vartheta\sin bt \end{pmatrix} \tag{16}$$

This state is a superposition of the two states that correspond to the anticrossing levels. In Chapter 5 we briefly discuss how to read out this mixture.

4. Three electrons: a very special Berry phase

In Figure 7 we show the avoided crossing that appears in the spectrum of $N = 3$, involving states with total angular momentum $J = M + S_z i = 3/2$. They are:

$$|S=3/2, M=3\, S_z=-3/2>, |S=1/2, M=2\, S_z=-1/2>, |S=1/2, M=1\, S_z=1/2>$$

The SU(3) Berry phase requires eight parameters to be available for the 3×3 hermitian Hamiltonian matrix. This is far too much for present fabrication possibilities. We have considered the possibility of controlling a smaller amount of degrees of freedom, which produces an accidental crossing of a third level in an otherwise SU(2) parameter manifold. The states given above are coupled by spin-orbit when the electric field is of the kind

$$E_z(t) = e + g_1(t)\cos\theta + g_2(t)\sin\theta \tag{17}$$

with $g_1 + ig_2 = |g|e^{i\omega t}$. In fact, they contain Slater determinants whose single particle states have non zero matrix elements of the spin orbit interaction between some constituents of single particle states.

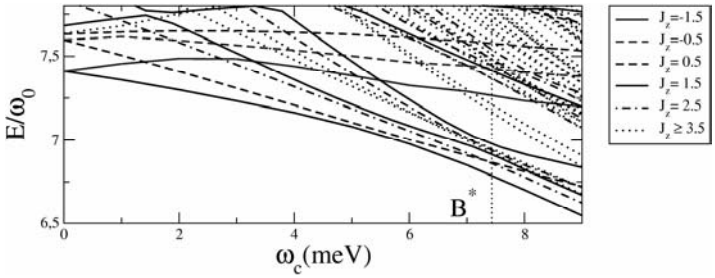

Fig. 7. A dot with $N = 3$ particles: energy spectrum vs. magnetic field ω_c in the presence of SO for $\omega_d = 7$ meV, $U = 13$ meV, and $\alpha = 250$ meV·Å. The GS is $J_z = 3/2$, the FES is $J_z = 5/2$

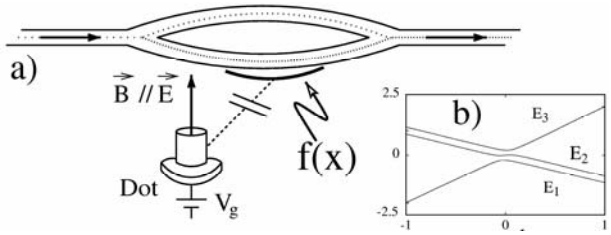

Fig. 8. A sketch of a possible experimental setup for detecting the Berry phase (a); $f(x)$ accounts for the spatial modulation of the coupling between the dot and interferometer (see text); energy levels of the dot, E_ℓ , vs. $b = (3/2)(B - B^*)$ (b)

Let us denote the relevant single particle states by the sequence of quantum numbers $(n, m, s = 1/2, s^z)$. The states $(1, \vec{\lambda}) \equiv (11, 1/2, -1/2, \vec{\lambda})$, $(3, \vec{\lambda}) \equiv (22, 1/2, -1/2, \vec{\lambda})$, and $(2, \vec{\lambda}) \equiv (11, 1/2, 1/2, \vec{\lambda})$ are present in some of the Slater determinants that form the many-body states given above and have non vanishing matrix elements of the spin orbit interaction of Eq. (17), according to the Hamiltonian:

$$\hat{h}[b, g_1, g_2, e] = \begin{bmatrix} -b & 0 & g^* \\ 0 & 2b & e \\ g & e & -b \end{bmatrix} \tag{18}$$

If $b = 3(B - B^*)/2$, the three eigenvalues become degenerate at $B = B^*$ and $E = 0$. $\hat{h}[b, g_1, g_2, e]$ is a traceless 3×3 Hermitian matrix, belonging to the SU(2)-algebra. Its eigenvalues take a simple form in terms of the "polar" coordinates R, Ψ

$$R = \sqrt{b^2 + \frac{e^2 + |g|^2}{3}}, \qquad \sin(3\Psi) = -\frac{b(b^2 + \frac{e^2}{2} - |g|^2)}{R^3} \tag{19}$$

In decreasing order, the energies are given by [17]:

$$E_\ell = 2R \sin\left[\Psi + \frac{2}{3}(\ell - 1)\pi\right], \quad \ell = 1, 2, 3 \tag{20}$$

In Figure 8b, we plot E_1, E_2 and E_3 versus b for small but nonzero e and g. The corresponding eigenvectors will be denoted further by $|e_\ell, \vec{\lambda}>$, $\ell = 1,2,3$. Figure 8b shows the avoided crossing vs. b. In particular, if $b < 0$, then the level E_1 is almost degenerate with E_2, and the degeneracy at $e = g = 0$ takes place at $\Psi = \pi/6$. On the other hand, if $b > 0$, then it is E_3 that is almost degenerate with E_2, and the degeneracy takes place at $\Psi = \pi/2$. At $b = 0$ an "exceptional" three-level degeneracy arises, when $e = g = 0$ ($R = 0$), which is not, however, an accidental three-level degeneracy.

The explicit calculation of the Berry phase for a closed path γ at fixed b, lying in the subspace of the coordinates (g_1, g_2, e), can be found in [17].

For $b < 0$, there is an energy gap of order b between E_3 and the next available energy level (E_2), so that we do not expect any Berry phase to arise within such a region. On the other hand, we do expect a Berry phase to appear for $b > 0$ when E_3 is almost degenerate with E_2. Therefore, whether the Berry phase arises or not is just a matter of whether $b > 0$ or $b < 0$. Clearly, no fine tuning of the external field is required, provided it is possible to move B across B^*.

Our realization of the Berry phase in a quantum dot is the simplest setup that can be theoretically studied retaining the required features. Actually, its experimental realization is quite demanding, at least as long as one is concerned with a single dot. For instance, one can imagine a setup where the maximum of E could be off-centre in the dot area and rotating in time. Alternatively, asymmetries in the shape of the dot that slowly depend on time might produce a Berry phase.

5. Comments on detecting the superposition of dot states

In conclusion, by applying a rather strong orthogonal magnetic field $B \perp z$, a disk shaped Quantum Dot (QD) with a few electrons becomes a droplet of maximum electron density (MDD), maximum total angular momentum M, and maximum spin S. An increase of S and M occurs via crossings between levels. A prototype of this occurrence is the singlet–triplet transition in a two-electron dot. A gate voltage induces the Rashba (spin-orbit) term, which couples S to the electric field orthogonal to the QD disk. M and S_z are no longer good quantum numbers, but $J_z = M + S_z$ is. This changes the crossing into an avoided crossing, because of the level repulsion between levels with equal J_z. We monitor these crossings for a dot with a few electrons by means of exact diagonalisation (up to $N = 5$ electrons). By operating the electric field, one can construct a superposition of the states involved in the anticrossing. Their phase is controlled by changing the applied electric field in time.

The level structure of the dot close to the anticrossing can be modelled by an effective spin Hamiltonian. We have studied an isolated QD at fixed N elsewhere [17], with a weak capacitive contact to one arm of a two path interferometer. By operating with a gate voltage on the dot cyclically in time, we have proposed to modulate the transmission across the interferometer (see Fig. 8). Electrons travelling in the edge states of the interferometer's arm that are coupled to the dot may feel the charge-

charge correlations at different times and be reflected by what looks like a change in the effective dielectric constant in time.

Here, we have discussed only the cases of $N = 2$ and $N = 3$, which show marked avoided crossings in the level structure versus B. At larger N , these features are smeared out substantially and a different physics takes over. A closer look at the QD energy spectrum shows that e-e correlations and spin-orbit produce a spin texture in the first excited state beyond B^*, with a reversed spin density concentrated at the origin [14]. The situation resembles a quantum Hall ferromagnet (QHF) with filling close to one. In the QHF, symmetry breaking due to full spin polarization sustains a gapless collective spin excitation, named the "skyrmion". In the QD, the gap is finite and it is tuned by the Rashba coupling. This opens up many unexpected possibilities of controlling electron spin density at the dot and the possibly underlying nuclear spins coupled via hyperfine interaction.

References

[1] DiVincenzo D.P., Science, 270 (1995), 255.
[2] Nakamura Y., Pashkin Y.A., Tsai J.S., Nature, 398 (1999), 768.
[3] Mooij J.E. Orlando T.P., Levitov L., Tian L., van der Wal C.H., Lloyd S., Science, 285 (1999), 1036.
[4] Bayer M., Hawrylak P., Hinzer K., Fafard S., Korkusinski M., Wasilewski Z.R., Stern O., Forchel A., Science, 291 (2001), 451; Petta J.R., Johnson A.C., Marcus C.M., Hanson M.P., Gossard A.C., Phys. Rev. Lett., 93 (2004), 186802.
[5] Schliemann J., Loss D., MacDonald A.H., Phys. Rev. B, 63 (2001), 085311.
[6] Kastner M.A., Ann. Phys., 9 (2000), 885; Sasaki S., de Franceschi S., Elzerman J.M., van der Wiel W.G., Eto M., Tarucha S., Kouwenhoven L.P., Nature, 405 (2000), 764.
[7] Farhi E., Goldstone J., Guthann S., Lapan J., Lundgren A., Preda D., Science, 292 (2001), 472; Pachos J., Zanardi P., Rasetti M., Phys. Rev. A, 61 (2000), 010305(R).
[8] Jouault B., Santoro G., Tagliacozzo A., Phys. Rev. B, 61 (2000), 10242; Kouwenhoven L.P., Oosterkamp T.H., Danoesastro M.W., Eto M., Austing D.G., Honda T., Tarucha S., Science, 278 (1997), 1788.
[9] Berry M.V., Proc. R. Soc. London, Ser. A, 392 (1984), 45.
[10] Merkt U., Huser J., Wagner M., Phys. Rev. B, 43 (1991), 7320; Tarucha S., Austing D.G., Honda T., van der Hage R.J., Kouwenhoven L.P., Phys. Rev. Lett., 77 (1996), 3613.
[11] Oosterkamp T.H., Janssen J.W., Kouwenhoven L.P., Austing D.G., Honda T., Tarucha S., Phys. Rev. Lett., 82 (1999), 2931.
[12] Rokhinson L.P., Guo L.J., Chou S.Y., Tsui D.C., Phys. Rev. Lett., 87 (2001), 166802.
[13] Chamon C. de C., Wen X.G., Phys. Rev. B, 49 (1994), 8227; Reimann S.M., Koskinen M., Manninen M., Mottelson B.R., Phys. Rev. Lett., 83 (1999), 3270.
[14] Lucignano P., Jouault B., Tagliacozzo A., Phys. Rev. B, 69 (2004), 045314.
[15] Lucignano P., Jouault B., Tagliacozzo A., Altshuler B., to be published.
[16] Pustilnik M., Glazman L.I., Phys. Rev. Lett., 85 (2000), 2993; Eto M., Nazarov Y., Phys. Rev. Lett., 85 (2000), 1306; Pustilnik M., Avishai Y., Kikoin K., Phys. Rev. Lett., 84 (2000), 1756.
[17] Giuliano D., Sodano P., Tagliacozzo A., Phys. Rev. B, 67 (2003), 155317.

Received 20 September 2004
Revised 9 November 2004